Available online at www.sciencedirect.com

ScienceDirect

Ceramics International 40 (2014) 117–122

CERAMICS INTERNATIONAL

www.elsevier.com/locate/ceramint

Effects of simultaneous change of Mg^{2+} and Ti^{4+} contents on the luminescence properties of $Y_2O_2S:Eu^{3+}$, Mg^{2+}, Ti^{4+} nanotubes

Dan Liu[a], Ping Huang[a], Cai'e Cui[a,b,*], Lei Wang[a,b], Guowei Jiang[a]

[a]Physics and Optoelectronic Engineering College, Taiyuan University of Technology, Taiyuan, Shanxi 030024, PR China
[b]Observation and Control Technology Research Institute, Taiyuan University of Technology, Taiyuan, Shanxi 030024, PR China

Received 18 April 2013; received in revised form 25 April 2013; accepted 29 May 2013
Available online 4 June 2013

Abstract

Red long-lasting phosphor $Y_2O_2S:Eu^{3+}$, Mg^{2+}, Ti^{4+} nanotubes were synthetized by the hydrothermal method. The effects of simultaneous change of Mg^{2+} and Ti^{4+} contents on the luminescence properties were investigated. The samples were characterized by powder X-ray diffraction (XRD), scanning electron microscopy (SEM), photoluminescence (PL), and thermoluminescence spectra (TL). XRD investigation revealed that the precursors was a pure phase of $Y(OH)_3$ and the sulfuretted samples was a pure phase Y_2O_2S. SEM observation showed that the sulfuretted phosphors inherited the tube-like shape from the precursors. Under 325 nm UV excitation, the samples exhibited the strongest red emission at 627 nm, which corresponded to the transition from $^5D_0$ to $^7F_2$ level of Eu^{3+} ion. When the content of (Mg^{2+}, Ti^{4+}) multiple-ion dopant was 3.0%, the trap depth of sample was 0.9 eV and the decay time could last for over 450 s (≥1 mcd/m^2) after 365 nm UV radiation for 10 min.

Keywords: $Y_2O_2S:Eu^{3+}$, Mg^{2+}, Ti^{4+}; Nanotubes; Luminescence

1. Introduction

Recently, low-dimensional long-lasting phosphor materials have attracted great attention because their luminescence properties can be greatly affected by the dimensions and morphology, and such phosphor materials have been widely applied in optical, electronic, biochemical, and medical devices [1–5]. Up to now, much work has been done in this field. During the research, there are some methods for preparation of fine powders in nanosize, such as the sol–gel method, chemical precipitation, the hydrothermal method, and so on. The hydrothermal method which exhibits some advantages of low processing temperature, high homogeneity, and crystal shape easily controlled has become a promising method for the synthesis of well-crystallized nanomaterials. A great many nanocrystal phosphors with controlled morphology have been synthesized, such as many kinds of rare earth oxides and hydroxides, Y_2O_3, Eu_2O_3, $Y(OH)_3$, $Eu(OH)_3$, $La(OH)_3$,$Gd(OH)_3$ and so on [6–9]. As for rare earth oxysulfide materials, Y_2O_2S, Gd_2O_2S, Eu_2O_2S and La_2O_2S are known as nanorods [10], La_2O_2S and Nd_2O_2S as nanowires [11] and Y_2O_2S as nanotubes [6].

The long-lasting phosphor $Y_2O_2S:Eu^{3+}$, Mg^{2+}, Ti^{4+} has been known as the best red luminescent material at present. In Y_2O_2S host, Mg^{2+} and Ti^{4+} substitute the site of Y^{3+}, which results in defects where electrons and/or holes can be trapped into. Following the Kröger–Vink notation, Mg^{2+} in the Y^{3+} site will create an Mg'_Y defect with a negative net charge and compensated by an oxygen vacancy V''_O Eq. (1). Ti^{4+} co-doping will create a positive defect (Ti'_Y) compensated by an interstitial oxide ion (O'_i) [12].

$$2Y^{3+} \rightarrow 2Mg'_Y + V''_O \quad (1)$$

$$2Y^{3+} \rightarrow 2Ti'_Y + O''_i \quad (2)$$

In this situation, to keep charge balance, $2Y^{3+}$ ions are replaced by $1Ti^{4+}$ and $1Mg^{2+}$ ion. Thus, the research of simultaneous change of Mg^{2+} and Ti^{4+} contents is very important for studying the luminescent mechanism on the $Y_2O_2S:Eu^{3+}$, Mg^{2+}, Ti^{4+} phosphor.

In this paper, the precursor $Y(OH)_3$: Eu^{3+}, Mg^{2+}, Ti^{4+} nanotubes has been prepared via the hydrothermal method. Then the precursor has been sulfuretted in CS_2 atmosphere to

*Corresponding author at: Physics and Optoelectronic Engineering College, Taiyuan University of Technology, Taiyuan, Shanxi 030024, PR China. Tel.: +86 351 4175 345.
E-mail address: tytgcejy@sina.com (C. Cui).

0272-8842/$ - see front matter © 2013 Elsevier Ltd and Techna Group S.r.l. All rights reserved.
http://dx.doi.org/10.1016/j.ceramint.2013.05.111

obtain the long afterglow phosphor $Y_2O_2S:Eu^{3+}$, Mg^{2+}, Ti^{4+} nanotubes. The effects of simultaneous change of Mg^{2+} and Ti^{4+} contents on the crystal characteristics, morphology, luminescent properties and afterglow performance of $Y_2O_2S:Eu^{3+}$, Mg^{2+}, Ti^{4+} phosphors are discussed.

2. Experimental

A tube-like $Y(OH)_3$ precursor, co-doped with Eu, Mg and Ti, was firstly prepared by the hydrothermal method. In a typical procedure, 10 ml 0.5 mol/l $Y(NO_3)_3$ solution, 3 ml 0.05 mol/l $Eu(NO_3)_3$ solution, 1 ml 0.05 mol/l $Mg(NO_3)_3$ solution and 1 ml 0.05 mol/l the dibutyl phthalate solution modified by the acetyl acetone were mixed to get a component with 100% Y^{3+}, 3% Eu^{3+}, 1% Mg^{2+} and 1% Ti^{4+} in mole ratio. And in the following, 14 ml deionized water and 7 ml absolute alcohol were added to form homogeneous mixture by stirring. Then 4 mol/l NaOH solution was added drop-wisely to the solution to generate a colloidal solution with a pH around 13. This colloidal solution was transferred to a Teflon-linked autoclave and maintained at 180 °C for 12 h. When the autoclave was cooled down to room temperature, the desired white $Y(OH)_3$: Eu^{3+}, Mg^{2+}, Ti^{4+} precipitations were collected, washed with deionized water four times, and finally dried at 80 °C. To investigate the effects of simultaneous change of Mg^{2+} and Ti^{4+} contents on the luminescence properties, we defined the content of (Mg^{2+}, Ti^{4+}) multiple-ion dopant as X ($X=1.0\%$, 2.0%, 3.0%, 4.0%, and 5.0%), $Y(OH)_3:Eu^{3+}$ precursors with different X doping were systematically prepared in a similar way. Then these precursors were calcined at 750 °C for 6 h in CS_2 atmosphere which was formed by the reaction of sulfur and carbon. Finally, the precursors formed the tube-like long afterglow phosphors $Y_2O_2S:Eu^{3+}$, Mg^{2+}, Ti^{4+}.

The crystal structure of the products was detected by SHIMADZU-6000 X-ray generator with Cu Kα ($\lambda=0.15406$ nm) radiation and the scan step was 0.02 °C. The PL spectra of the samples was measured by an F-280 spectrophotometer with a 150 W Xe lamp as excitation source. The morphology of the powders was observed by employing scanning electron microscopy (Hitachi S-4800FESEM). The afterglow properties were collected using the brightness meter (ST-86LA) with the help of a stopwatch. TL spectra of samples were measured on a model FJ-427A1TL meter with a heating rate of 1 K/s from room temperature to 673 K. The samples were excited for 10 min by 365 nm UV radiation standard lamp with a power of 6 W before measuring their TL curves and the afterglow properties. All measurements were carried out at room temperature except for the TL curves.

3. Results and discussion

3.1. Phase characterization

Fig. 1 indicates XRD patterns of $Y(OH)_3:Eu^{3+}$, Mg^{2+}, Ti^{4+} precursor with X for 3.0% and $Y_2O_2S:Eu^{3+}$, Mg^{2+}, Ti^{4+} with different dopant contents. In Fig. 1(a), it demonstrates that all peaks are in good agreement with the diffraction from

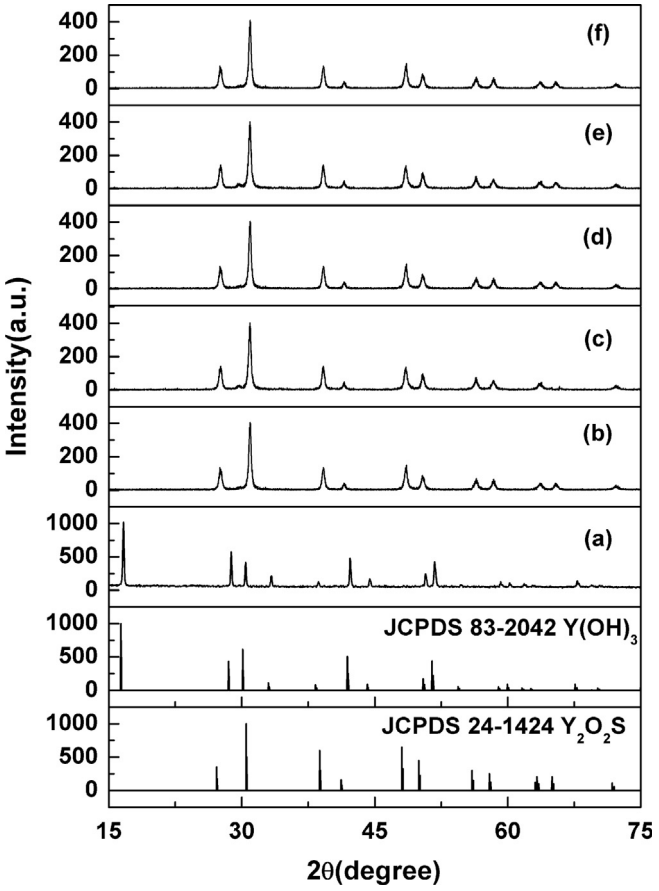

Fig. 1. XRD patterns of (a) $Y(OH)_3:Eu^{3+}$, Mg^{2+}, Ti^{4+} with X for 3.0% and $Y_2O_2S:Eu^{3+}$, Mg^{2+}, Ti^{4+} with different X: (b) 1.0%; (c) 2.0%; (d)3.0%; (e) 4.0%; and (f) 5.0%.

hexagonal $Y(OH)_3$ phase according to standard powder diffraction file, PDF # 83-2042, and no impurity is detected. By analyzing Fig. 1(b)–(f) curves, all peaks are in good agreement with the diffraction from hexagonal Y_2O_2S structure (space group $P\bar{3}$ m1, No. 164, $Z=1$, with $a=3.784$ Å and $c=6.589$ Å), which are very close to the standard lattice parameters provided by the powder diffraction file, PDF # 24-1424. No impure peaks are observed, demonstrating that the substitution of Y^{3+} with trace Mg^{2+} and Ti^{4+} do not remarkably change the crystal structure and lattice parameters of $Y(OH)_3$ and Y_2O_2S.

3.2. Morphology of $Y(OH)_3:Eu^{3+}$, Mg^{2+}, Ti^{4+} precursors and $Y_2O_2S:Eu^{3+}$, Mg^{2+}, Ti^{4+} phosphors

Fig. 2 presents the SEM images of $Y(OH)_3:Eu^{3+}$, Mg^{2+}, Ti^{4+} and $Y_2O_2S:Eu^{3+}$, Mg^{2+}, Ti^{4+} with X for 3.0%. As can be seen in Fig. 2(a), the morphology of $Y(OH)_3:Eu^{3+}$, Mg^{2+}, Ti^{4+} precursors is tube-like structure, and the length of nanotubes is several micrometers and the diameter is 80–150 nm. In Fig. 2 (b), for $Y_2O_2S:Eu^{3+}$, Mg^{2+}, Ti^{4+} phosphors, their 1D linear morphology and diameters are nearly identical to those of the initial $Y(OH)_3$: Eu^{3+}, Mg^{2+}, Ti^{4+} precursors, implying that the tube-like shape is kept after calcining for 6 h at 750 °C in CS_2

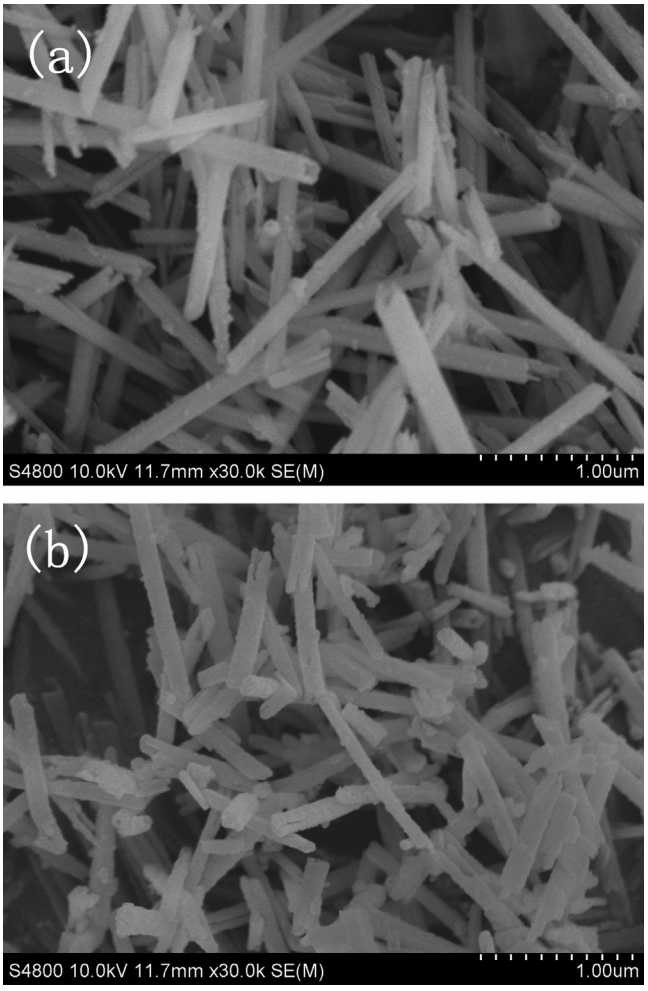

Fig. 2. SEM images of (a) $Y(OH)_3$:Eu^{3+}, Mg^{2+}, Ti^{4+} and (b) Y_2O_2S:Eu^{3+}, Mg^{2+}, Ti^{4+}.

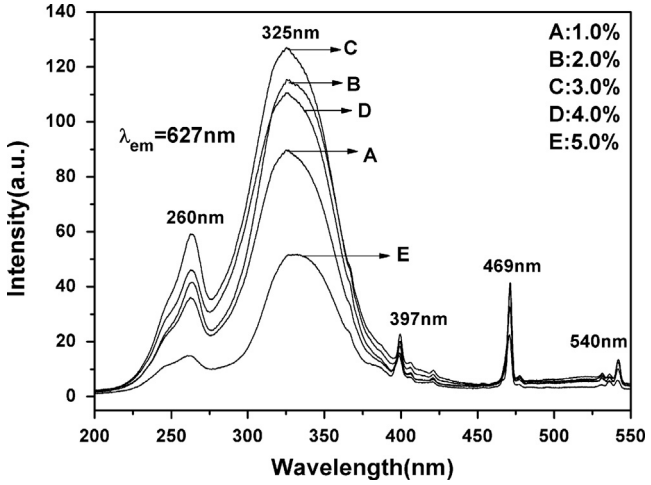

Fig. 3. The excitation spectrums of Y_2O_2S:Eu^{3+}, Mg^{2+}, Ti^{4+} nanotubes with different dopant contents.

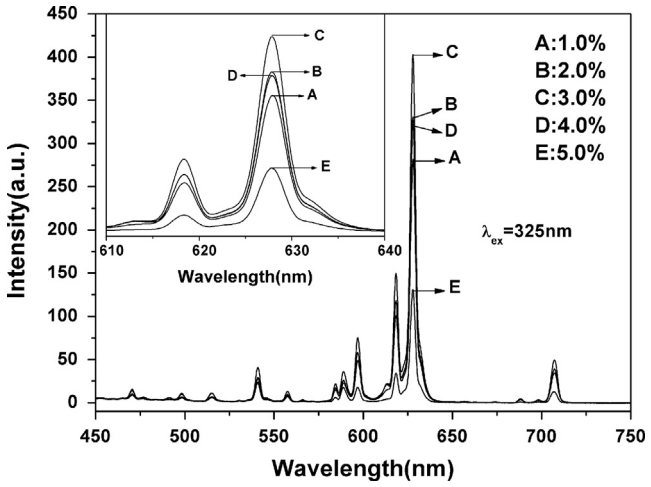

Fig. 4. The emission spectra of Y_2O_2S:Eu^{3+}, Mg^{2+}, Ti^{4+} nanotubes with different dopant contents (the inset picture shows the enlarged emission spectra within 610—640 nm).

atmosphere. Therefore, the tube-like Y_2O_2S:Eu^{3+}, Mg^{2+}, Ti^{4+} can be easily prepared by such facile routine in lower temperature.

3.3. Luminescence spectra of Y_2O_2S:Eu^{3+}, Mg^{2+}, Ti^{4+} nanotubes

Fig. 3 indicates the excitation spectra of Y_2O_2S:Eu^{3+}, Mg^{2+}, Ti^{4+} nanotubes with different dopant contents. Fig. 3 shows that there is a wild band with two peaks at about 260 and 325 nm, due to the Eu^{3+}-O^{2-} CTB (charge transfer band) and Eu^{3+}-S^{2-} CTB respectively. The S^{2-} (3p)→Eu^{3+}charge transfer band probably overlaps with the energy transfer Ti→Eu^{3+} which is a consequence of the charge transfer transition Ti^{4+}+e^- (O^{2-} (2 P))→Ti^{3+} and subsequent energy transfer to Eu^{3+}. Weaker peaks between 380 nm and 550 nm are attributed to the $^7F_{0,1}$→$^5D_{1,2,3}$ transitions of Eu^{3+} [13].

The emission spectra of Y_2O_2S:Eu^{3+}, Mg^{2+}, Ti^{4+} nanotubes with different dopant contents is shown in Fig. 4. When the samples are excited under 325 nm UV light, all of spectral lines are in agreement with the intrinsic emission of Eu^{3+}, the strong peaks at 627 nm and 617 nm are because of the $^5D_0$→$^7F_2$ transition of Eu^{3+}, and some weak and narrow peaks at 450–750 nm are attributed to the $^5D_{1,2}$→^7F_J(J=0–4) transitions of Eu^{3+} [13,14]. The result shows that the samples doped with Mg^{2+} and Ti^{4+} ions do not change the position of emission peaks of Eu^{3+}.

According to the fluorescence spectra, when the Y_2O_2S:Eu^{3+}, Mg^{2+}, Ti^{4+} phosphor is doped with 3.0% of (Mg^{2+},Ti^{4+}) multiple-ion, the intensity of excitation spectra observed reaches the maximum value. While dopant content is over 3.0%, the intensity is decreased. Thus, it is also suggested that the optimized dopant content is 3.0%, which is in agreement with the result of emission spectra. The result may be explained as the following: among several luminescence transitions of Eu^{3+}, the $^5D_0$→$^7F_1$(~590 nm) emission transition is mainly a magnetic-dipole transition. It is structure independent while $^5D_0$→$^7F_2$ (627 nm) and $^5D_0$→$^7F_4$ (~700 nm) are hypersensitive forced and weak electric–dipole transitions, respectively, being allowed only at low

symmetries with no inversion center. These transitions are known to be hypersensitive to crystal-structure and chemical surroundings [15]. In Y_2O_2S host, Eu^{3+} substitutes the site of Y^{3+}, while Y^{3+} ions occupy the center of no inversion symmetry, making no inversion symmetry reinforced. Therefore, the emission of $Y_2O_2S:Eu^{3+}$ at 627 nm and 617 nm is the strong peaks. Mg^{2+} and Ti^{4+} ions also play the same role. Firstly, no inversion symmetry is reinforced along with the increase of dopant content and luminescent intensity is raised. But when the dopant content exceeds 3.0%, it will make no inversion symmetry weaken and symmetries reinforced, so the luminescent property becomes poor.

3.4. Afterglow decay curves and TL curves of samples

The afterglow decay curves of $Y_2O_2S:Eu^{3+}$, Mg^{2+}, Ti^{4+} nanotubes with different dopant contents after irradiation with 365 nm UV light for 10 min are shown in Fig. 5. The decay behavior of $Y_2O_2S:Eu^{3+}$, Mg^{2+}, Ti^{4+} nanotubes shows a rapid decay at the beginning and then a stable long persistent process. However, the phosphor shows different afterglow properties with different dopant contents. The initial brightness and afterglow time of the phosphor show the tendency firstly increases then decreases gradually with dopant content. When dopant content is 3.0%, the afterglow phosphor $Y_2O_2S:Eu^{3+}$, Mg^{2+}, Ti^{4+} nanotubes exhibits the highest initial brightness and the longest afterglow time, which are 960 mcd/m^2 and 450 s (≥1 mcd/m^2), respectively. The afterglow mechanism can be explained by the contribution from the electron traps formed by the co-doped Mg^{2+} and Ti^{4+}.They occupy the same lattice sites as Y^{3+} ions do. To keep charge balance, $2Y^{3+}$ ions are replaced by $1Ti^{4+}$ and $1Mg^{2+}$ ion. However, such replacement breaks the charge balance around local lattice site and causes the formation of new electronic donating and accepting levels between the host lattice band gaps, an excessive positive charge which serves as the electron trap around the doped Ti^{4+} ion is created. Then one of the two kinds of ions absorbs energy and thermally transfers to Eu^{3+} ions which serve as trap centers. The trap of stored energy which is constituted by Ti^{4+} and Mg^{2+} ions serves as donor leveling and Eu^{3+} serves as acceptor leveling. The trapping of excited electrons and thermally released processes cause the appearance of afterglow [16].

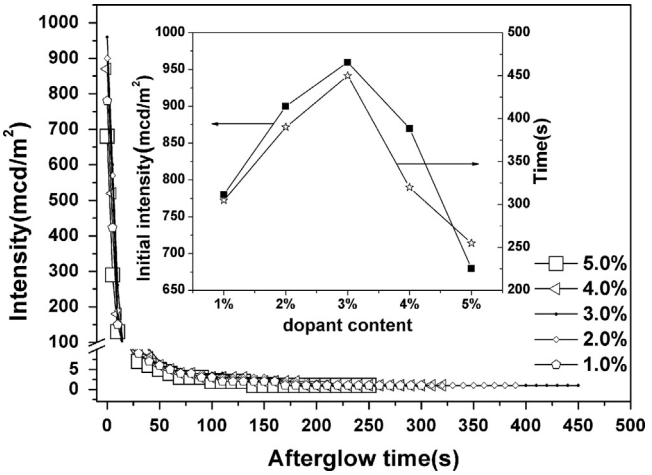

Fig. 5. The afterglow decay curves of phosphors with different dopant contents (the inset picture shows the initial intensity and afterglow time of phosphors with different dopant contents).

Since the persistent luminescence is the hole trapped-transported-detrapped process, so the afterglow characteristics of the phosphors are affected greatly by the frequency factor, the depth and the density of traps [17–19]. In order to investigate the effect of different contents of (Mg^{2+}, Ti^{4+}) multiple-ion dopant on the long-lasting phosphor $Y_2O_2S:Eu^{3+}$, Mg^{2+}, Ti^{4+} nanotubes, TL spectrum is used. Fig. 6 indicates the TL curves of the samples with different dopant contents after irradiation with 365 nm UV radiation for 10 min. From the report [20], the TL peaks are located in the region of 323–383 K where it is beneficial for the appearance of afterglow. In Fig. 6, all peaks are located in this region. With the increase of dopant content, the intensity of TL peak is increased gradually. And when dopant content is 3.0%, the intensity of TL peak reaches maximum, implying that moderate content of (Mg^{2+}, Ti^{4+}) multiple-ion dopant can improve the trap density. But when dopant content exceeds 3.0%, the intensity of TL peak begins to decrease because concentration quenching occurs [21].

In order to explain the influence of the depth of trap energy levels in samples, the corresponding trapping parameters can be estimated by analyzing the TL peak using the equation

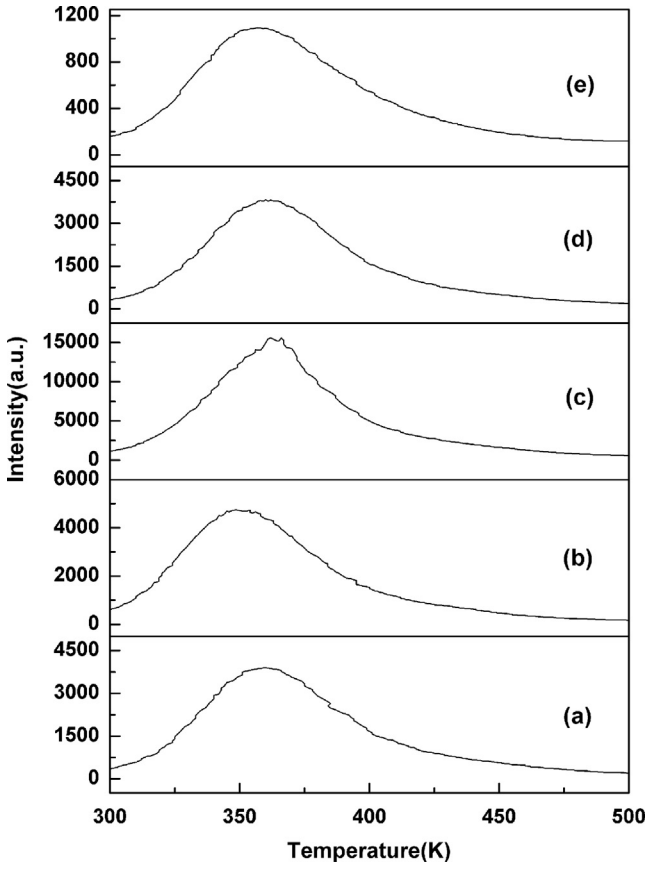

Fig. 6. The TL curves of phosphors $Y_2O_2S:Eu^{3+}$, Mg^{2+}, Ti^{4+} nanotubes with different dopant contents: (a) 1.0%; (b) 2.0%; (c) 3.0%; (d) 4.0%; (e) 5.0%.

Table 1
Trapping parameters of $Y_2O_2S:Eu^{3+}$, Mg^{2+}, Ti^{4+} nanotubes for different dopant contents.

X (%)	T_m/K	T_2/K	E/eV
1.0	360	395	0.64
2.0	354	384	0.72
3.0	362	387	0.90
4.0	360	394	0.68
5.0	358	399	0.54

given by the Lushchik method [20].

$$E = 2k(T_m)^2/(T_2-T_m) \quad (3)$$

where T_m is the peak temperature, $T_2$is the temperature value which corresponds to the point on the right side of the TL curve, where the peak intensity is half of the peak value, $k$is the Boltzmann's constant. The related parameters are calculated using Eq. (3) and listed in Table 1.

In order to achieve long lasting phosphorescence, the trapping levels need to locate at a suitable depth. If the trap level is too shallow, only small amount of electrons can be captured to traps. Under the action of thermal disturbances, electrons are easily released from traps and then combined with holes in the g round state, which results in shorter afterglow time. On the other hand, if the trap level is too deep, the captured electrons will be hard to return to the excited state levels at room temperature, which also results in poor afterglow property. From Fig. 6 and Table 1, the sample doped with 3.0% of (Mg^{2+}, Ti^{4+}) multiple-ion dopant has the maximum intensity of TL peak and the deepest trap depth with 0.90 eV, and it shows the optimal initial luminance and afterglow time. From Fig. 6 and Table 1, for the phosphor $Y_2O_2S:Eu^{3+}$, Mg^{2+}, Ti^{4+}, the high trap density and deep trap depth is suitable to produce optimal afterglow properties.

4. Conclusions

Red long-lasting phosphor $Y_2O_2S:Eu^{3+}$, Mg^{2+}, Ti^{4+} nanotubes with different contents of (Mg^{2+}, Ti^{4+}) multiple-ion dopant are prepared through the hydrothermal method combining with a post-calcining process. Pure phase of $Y(OH)_3$ and Y_2O_2S can be obtained during the experiment. The morphology of the $Y_2O_2S:Eu^{3+}$, Mg^{2+}, Ti^{4+} phosphors inherits the tube-like shape from the precursors after calcinating for 6 h at 750 °C in CS_2 atmosphere. The $Y_2O_2S:Eu^{3+}$, Mg^{2+}, Ti^{4+} nanotubes has strong red-emission lines at 627 nm which ascribes to the transition from $^5D_0$ to $^7F_2$ level of Eu^{3+} ion under the 325 nm UV irradiation. While the sample doped with 3.0% of (Mg^{2+}, Ti^{4+}) multiple-ion dopant has the highest trap density and the deepest trap depth, which leads to the optimal initial luminance and afterglow time. Therefore, for red long-lasting phosphor $Y_2O_2S:Eu^{3+}$, Mg^{2+}, Ti^{4+} nanotubes, the optimal content of (Mg^{2+}, Ti^{4+}) multiple-ion dopant is 3.0%.

Acknowledgments

This present work was financially supported by the National Natural Science Foundation of China (No. 51072128), Key Research Project of Science and Technology of Shanxi (No. 20110321040-01) and Program for the Top Young Academic Leaders of Higher Learning Institutions of Shanxi.

References

[1] J.Y. Kuang, Y.L. Liu, J.X. Zhang, White-light-emitting long-lasting phosphorescence in Dy^{3+}-doped $SrSiO_3$, Journal of Solid State Chemistry 179 (2006) 266.
[2] X. Wang, J. Zhang, Q. Peng, Y.D. Li, A general strategy for nanocrystal synthesis, Nature 437 (2005) 121.
[3] B.C. Cheng, H.J. Liu, M. Fang, Y.H. Xiao, S.J. Lei, L.D. Zhang, Long-persistent phosphorescent $SrAl_2O_4:Eu^{2+}$, Dy^{3+} nanotubes, Chemistry Communications, 8, 944–946.
[4] H.Y. Chen, M.H Weng, S.J. Chang, R.Y. Yang, Preparation of Sr2SiO4: Eu^{3+} phosphors by microwave-assisted sintering and their luminescent properties, Ceramics International 38 (2012) 125–130.
[5] B.C. Cheng, L.T. Fang, Z.D. Zhang, Y.H. Xiao, S.J. Lei, $BaAl_2O_4:Eu^{2+}$, Dy^{3+} Nanotube Synthesis by Heating Conversion of Homogeneous Coprecipitates and Afterglow Characteristics, Journal of Physical Chemistry C 115 (2011) 1708–1713.
[6] X Wang, Y.D. Li, Synthesis and characterization of lanthanide hydroxide single-crystal nanowires, Angewandte Chemie International Edition 41 (2002) 4790.
[7] X. Wang, X.M. Sun, D.P. Yu, B.S. Zou, Y.D. Li, Rare earth compound nanotubes, Advanced Materials 15 (2003) 1442–1445.
[8] G. Jia, K. Liu, Y.H. Zheng, Y.H. Song, M. Yang, H.P. You, Highly uniform $Gd(OH)_3$ and $Gd_2O_3:Eu^{3+}$ nanotubes: facile synthesis and luminescence properties, Journal of Physical Chemistry C 113 (2009) 6050–6055.
[9] Y.B. Mao, J.Y. Huang, R. Ostroumov, K.L. Wang, J.P. Chang, Synthesis and luminescence properties of erbium-doped Y_2O_3 nanotubes, Journal of Physical Chemistry C 112 (2008) 2278.
[10] S.P. Mao, Q. Liu, M. Gu, D.L. Mao, C.K. Chang, Long lasting phosphorescence of $Gd_2O_2S:Eu,Ti,Mg$ nanorods via a hydrothermal routine, Journal of Alloys and Compounds 465 (2008) 367.
[11] Y.Z. Huang, L. Chen, L.M. Wu, Crystalline nanowires of Ln_2O_2S, $Ln_2O_2S_2$, LnS_2 (Ln=La, Nd), and $La_2O_2S:Eu^{3+}$. Conversions via the Boron-Sulfur method that preserve shape, Crystal Growth and Design 8 (2008) 739.
[12] J. Hölsä, T. Laamanen, M. Lastusaari, M. Malkamäki, J. Niittykoski, E. Zych, Effect of $Mg^{2+}$and Ti^{IV} doping on the luminescence of $Y_2O_2S:Eu^{3+}$, Optical Materials, 31, 1791–1793.
[13] C.E. Cui, X. Lei, P. Huang, L. Wang, F. Yang, Influence of sulfuretted temperature on the luminescent properties of $Y_2O_2S:Eu^{3+}$, Mg^{2+}, Ti^{4+} nanoarrays, Journal of Luminescence 138 (2013) 138–142.
[14] P.F. Ai, W .Y. Li, L.Y. Xiao, Y.D. Li, H.J. Wang, Y.L. Liu, Monodisperse nanospheres of yttrium oxysulfide: synthesis, characterization, and luminescent properties, Ceramics International 36 (2010) 2169–2174.
[15] J. Thirumalai, R. Chandramohan, S. Auluck, T. Mahalingam, S.R. Srikumar, Controlled synthesis, optical and electronic properties of Eu^{3+} doped yttrium oxysulfide (Y_2O_2S) nanostructures, Journal of Colloid and Interface Science 336 (2009) 889–897.
[16] P. Huang, F. Yang, C.E. Cui, L. Wang, X. Lei, Luminescence improvement of $Y_2O_2S:Tb^{3+}$, Sr^{2+}, Zr^{4+} white-light long-lasting phosphor via Eu^{3+} addition, Ceramics International 39 (2013) 5615–5621.
[17] L. Jing, C.K. Chang, D.L. Mao, B. Zhang, A new long persistent blue-emitting $Sr_2ZnSi_2O_7:Eu^{2+}$,Dy^{3+} prepared by sol–gel method, Materials Letters 58 (2004) 1825–1829.

[18] T. Aitasalo, P. Dereń, J. Hölsä, H. Jungner, J.C. Krupa, M. Lastusaari, J. Legendziewicz, J. Niittykoski, W. Stręk, Persistent luminescence phenomena in materials doped with rare earth ions, Journal of Solid State Chemistry 171 (2003) 114–122.

[19] P. Huang, Y.Q. Wu, C.E. Cui, J. Guo, Enhancement of luminescence and afterglow in $Ca_{0.8}Zn_{0.2}TiO_3:Pr^{3+}$ by Nb^{5+} substitution for Ti^{4+}, Journal of Rare Earths 30 (2012) 100–104.

[20] S.Q. Deng, Z.P. Xue, Y.L. Liu, B.F. Lei, Y. Xiao, M.T. Zheng, Synthesis and characterization of $Y_2O_2S:Eu^{3+}$, Mg^{2+}, Ti^{4+} hollow nanospheres via a template-free route, Journal of Alloys and Compounds 542 (2012) 207–212.

[21] S.W.S. Mckeever, Thermoluminescence of Solids, Cambridge University Press, New York150–151.